NIH Public Access
Author Manuscript
J Am Chem Soc. Author manuscript; available in PMC 2012 June 8.

Published in final edited form as:
J Am Chem Soc. 2011 June 8; 133(22): 8606–8616. doi:10.1021/ja2004158.

A Targetable Fluorescent Sensor Reveals that Copper-Deficient *SCO1* and *SCO2* Patient Cells Prioritize Mitochondrial Copper Homeostasis

Sheel C. Dodani[1], **Scot C. Leary**[3], **Paul A. Cobine**[4], **Dennis R. Winge**[5], and **Christopher J. Chang**[*,1,2]

[1]Department of Chemistry, University of California, Berkeley, California 94720, United States

[2]Howard Hughes Medical Institute, University of California, Berkeley, California 94720, United States

[3]Department of Biochemistry, University of Saskatchewan, Saskatoon, SK S7N 5E5, Canada

[4]Department of Biological Sciences, Auburn University, Auburn, Alabama 36849, United States

[5]Department of Medicine and Biochemistry, University of Utah Health Sciences Center, Salt Lake City, Utah 84132, United States

Abstract

We present the design, synthesis, spectroscopy, and biological applications of Mitochondrial Coppersensor-1 (Mito-CS1), a new type of targetable fluorescent sensor for imaging exchangeable mitochondrial copper pools in living cells. Mito-CS1 is a bifunctional reporter that combines a Cu^+-responsive fluorescent platform with a mitochondrial-targeting triphenylphosphonium moiety for localizing the probe to this organelle. Molecular imaging with Mito-CS1 establishes that this new chemical tool can detect changes in labile mitochondrial Cu^+ in a model HEK 293T cell line as well as in human fibroblasts. Moreover, we utilized Mito-CS1 in a combined imaging and biochemical study in fibroblasts derived from patients with mutations in the two synthesis of cytochrome *c* oxidase 1 and 2 proteins (SCO1 and SCO2), each of which is required for assembly and metallation of functionally active cytochrome *c* oxidase (COX). Interestingly, we observe that although defects in these mitochondrial metallochaperones lead to a global copper deficiency at the whole cell level, total copper and exchangeable mitochondrial Cu^+ pools in *SCO1* and *SCO2* patient fibroblasts are largely unaltered relative to wildtype controls. Our findings reveal that the cell maintains copper homeostasis in mitochondria even in situations of copper deficiency and mitochondrial metallochaperone malfunction, illustrating the importance of regulating copper stores in this energy-producing organelle.

Introduction

Copper is a required element for life, and regulating its uptake, efflux, and compartmentalization at the cellular level is vital for maintaining normal physiology.[1-3] As such, cells have evolved intricate mechanisms that coordinate the activity of transporters, chaperones, and small-molecule ligands to dynamically control the distribution of copper within discrete subcellular spaces.[4-24] In this context, mitochondria are important reservoirs

* chrischang@berkeley.edu .

Supporting Information Available: Additional imaging and biochemical data and full reference information. This information is available free of charge via the Internet at http://pubs.acs.org.

NIH-PA Author Manuscript
NIH-PA Author Manuscript
NIH-PA Author Manuscript

NIH-PA Author Manuscript

NIH-PA Author Manuscript

NIH-PA Author Manuscript

for cellular copper owing to the essential role of this metal ion as a cofactor for the respiratory enzyme cytochrome *c* oxidase (COX), which reduces oxygen to water in the terminal step of aerobic respiration.[25-30] In addition to the copper present in COX, mitochondria utilize this metal ion as a cofactor for superoxide dismutase (SOD1) contained within the mitochondrial intermembrane space (IMS), and a matrix-localized pool of copper is relocalized to the IMS to metallate both of these enzymes.[31] Assembly of active COX in mitochondria requires a host of proteins, including the two synthesis of cytochrome *c* oxidase genes (*SCO1* and *SCO2*) that collectively mediate a series of metal- and redox-dependent events crucial for COX metallation and holoenzyme maturation.[32-44] Mutations in either of the SCO chaperones result in severe, tissue-specific clinical phenotypes that are caused by both a failure to mature functionally active COX for aerobic respiration, and an inability to appropriately regulate cellular copper homeostasis.[36,45-59]

Because regulating mitochondrial copper homeostasis is critical to maintaining central oxygen metabolism in the cell, new chemical tools that allow direct, real-time visualization of exchangeable mitochondrial copper pools in living samples are potentially powerful reagents with which to directly investigate the spatiotemporal distribution of this redox-active metal in both healthy and disease states. Towards this end, we have initiated a broad-based program to create fluorescent and MRI agents for monitoring labile copper stores in living systems.[60-68] Previous work from our laboratory on fluorescent sensors for live-cell copper imaging include intensity and ratiometric probes Coppersensor-1 (CS1)[60,61], Coppersensor-3 (CS3)[68], and Ratio-Coppersensor-1 (RCS1)[67], that are capable of selectively tracking labile cellular Cu^+ stores with metal and/or redox stimulation. However, these first-generation sensors and other elegant examples of small molecule or protein-based copper sensors[69-71] are not preferentially directed to mitochondria or other organelles, which offers an opportunity to devise new probes that can be targeted to discrete subcellular compartments for imaging local changes in the abundance/availability of exchangeable Cu^+.

In this report we present the design, synthesis, spectroscopy, and biological applications of Mitochondrial Coppersensor-1 (Mito-CS1), a new type of fluorophore for imaging dynamic mitochondrial copper stores in living cells with metal ion and spatial specificity (Scheme 1). Mito-CS1 can reversibly detect endogenous, exchangeable mitochondrial Cu^+ pools in a model HEK 293T cell line as well as in cultured human fibroblasts. Moreover, we apply Mito-CS1 in a combined molecular imaging and biochemical study to investigate mitochondrial copper homeostasis in fibroblasts derived from patients with *SCO1* and *SCO2* mutations. Interestingly, the data establish that although loss of function mutations in *SCO1* and *SCO2* cause a severe, global copper deficiency at the whole cell level, both the exchangeable Cu^+ and total mitochondrial copper pools are only mildly perturbed in *SCO1* and *SCO2* patient fibroblasts compared to wildtype congeners. Our results show that the cell maintains the homeostatic regulation of copper within mitochondria, even when faced with a globally severe state of copper deficiency, and underscore the primary importance of this redox-active metal in central metabolism and cellular energy homeostasis.[72]

Results and Discussion

Design and Synthesis of a Targetable Coppersensor Platform and Preparation of Mito-CS1

In order to monitor labile mitochondrial copper pools in living cells by real-time fluorescence imaging, we designed a bifunctional BODIPY dye that contains both a fluorescence-responsive Cu^+-binding domain and a mitochondrial-targeting moiety. For the latter, we exploited phosphonium head groups that have been pioneered by Murphy[73-76] and subsequently utilized by ourselves[77,78] and others[79-84] to selectively direct attached cargo to mitochondria via their proton gradients. In addition, we designed a synthetic pathway that builds up to one key intermediate, Carboxy-CS1, that combines a BODIPY chromophore, a

NIH-PA Author Manuscript

NIH-PA Author Manuscript

NIH-PA Author Manuscript

thioether-rich receptor for selective recognition and binding of Cu^+, and a carboxylic acid synthetic handle (Scheme 1, compound **9**) for facile introduction of a triphenylphosphonium tag or any other desired targeting functionality. We note that modification of the BODIPY chromophore to incorporate additional functionalities has been explored in the literature.[85,86]

Scheme 1 outlines the synthesis of Mito-CS1. Briefly, alkylation of aldehyde **1** with methyl bromoacetate furnishes the methyl ester **2** in 58% yield. Condensation of **2** with excess pyrrole and catalytic trifluoroacetic acid affords dipyrromethane **3** in 19% yield. Subsequent chlorination followed by oxidation with *p*-chloranil gives the dichloro dipyrromethene **4** in 44% yield over two steps; because isolation of the putative dichloro dipyrromethane intermediate is low yielding, we found that a halogenation/oxidation protocol was more synthetically tractable. Boron insertion with $BF_3{\bullet}OEt_2$ generates the dichloro BODIPY **5** in 75% yield. Nucleophilic displacement with sodium methoxide yields **6**, which is then coupled to the azatetrathia receptor **7** to generate **8** in 56% yield. Ester hydrolysis of **8** under basic conditions yields Carboxy-CS1 **9**. Peptide coupling of **9** and the mitochondrial-targeted tag **10** with HATU delivers Mito-CS1 (**11**) in 48% yield. We note that these mild and robust coupling conditions allow for the potential introduction of other functional tags onto Carboxy-CS1, including ones that can be used to direct fluorescent copper sensors to other organelles and other subcellular targets and that the synthetic pathway towards Mito-CS1 generates a versatile set of precursor materials (compounds **3**, **5**, **6**, and **7**).

Spectroscopic Properties of Mito-CS1

The spectroscopic properties of Mito-CS1 were evaluated in aqueous media buffered to physiological pH (PBS, pH 7.4). Apo Mito-CS1 features one prominent optical band at 555 nm ($2.8 \times 10^4\ M^{-1}\ cm^{-1}$) with a shoulder at 520 nm and a corresponding emission maximum at 569 nm with weak fluorescence ($\Phi = 0.009$). Upon addition of Cu^+, the absorption spectrum of Cu^+-bound Mito-CS1 displays a single major visible absorption band at 550 nm ($2.6 \times 10^4\ M^{-1}\ cm^{-1}$). The fluorescence intensity of Mito-CS1 increases by ca. 10-fold ($\Phi = 0.05$, Figure 1a) with a slight blue shift of the emission maximum to 558 nm with 1 equivalent of Cu^+ added (Figure 1a, inset), similar in photochemical properties to the previously reported turn-on fluorescent sensor CS1[60] (Cu^+-bound $\Phi = 0.13$, 10-fold turn-on response) but with the added functionality of a targeting phosphonium moiety. Binding analysis using the method of continuous variations (Job's plot) indicates a 1:1 Cu^+:dye complex is responsible for the observed fluorescence enhancement (Figure 1b). These results demonstrate that Mito-CS1 can dynamically respond to changes in Cu^+ levels in aqueous media. The apparent K_d for the Mito-CS1:Cu^+ complex is $7.2(3) \times 10^{-12}$ M in PBS buffer at pH 7.4 (Figure 2a). Even in the presence of a lipophilic phosphonium cation, Mito-CS1 maintains its high selectivity for Cu^+ over other biologically relevant metal ions (Figure 2b). The fluorescence response of apo or Cu^+-bound Mito-CS1 is not affected by the presence of physiologically relevant concentrations of Ca^{2+}, Mg^{2+}, and Zn^{2+}. Moreover, other bioavailable divalent metal ions (Mn^{2+}, Fe^{2+}, Co^{2+}, Ni^{2+}, Cu^{2+}) do not induce a change in the emission intensity of the apo probe and do not interfere with the Cu^+ response. Finally, Mito-CS1 is selective for Cu^+ over Cu^{2+}, showing that this probe has metal and redox specificity.

Fluorescence Detection of a Labile Mitochondrial Cu^+ Pool in HEK 293T Cells Using Mito-CS1

With spectroscopic data establishing that Mito-CS1 can selectively respond to Cu^+ in aqueous solution, we turned our attention to evaluate Mito-CS1 in live-cell imaging assays using HEK 293T as a model cell line. First, we tested Mito-CS1 for its ability to localize to mitochondria. Accordingly, HEK 293T cells stained with 500 nM Mito-CS1 for 15 min at

NIH-PA Author Manuscript

NIH-PA Author Manuscript

NIH-PA Author Manuscript

37 °C show measurable levels of fluorescence in discrete subcellular locations as determined by confocal microscopy (Figure 3a, Figure S1a). Co-staining experiments with MitoTracker Deep Red, a commercially available mitochondrial tracker (Figure 3b), BODIPY FL C_5-ceramide, a marker for the trans-Golgi (Figure 3c), and LysoTracker Green DND-26, a lysosomal marker (Figure S1b), establish that the observed fluorescence from Mito-CS1 is localized to mitochondria in these live cells. Furthermore, nuclear staining with Hoechst 33342 indicates that the cells are viable throughout the imaging experiments (Figure 3d, Figure S1c).

We next tested whether Mito-CS1 was sensitive enough to detect basal levels of labile mitochondrial Cu^+ and whether it could respond to increases and/or decreases in the size of this pool. First, HEK 293T cells were cultured in growth media only or growth media supplemented with 300 μM $CuCl_2$ for 18 h to globally elevate intracellular copper stores and subsequently imaged by confocal microscopy (Figure 4a, 4b). As visualized by Mito-CS1, we observe that exchangeable mitochondrial Cu^+ levels rise by 34% with copper supplementation relative to control, indicating that Mito-CS1 can detect expansions in the mitochondrial Cu^+ pool (Figure 4d).[31] To evaluate whether Mito-CS1 can also report on decreases in exchangeable mitochondrial Cu^+ levels, HEK 293T cells were cultured in growth media only or growth media supplemented with 100 μM of the membrane-impermeable Cu^+ chelator bathocuproine disulfonate (BCS) for 18 h to globally deplete intracellular copper stores,[87] and each set of cells were then stained with Mito-CS1 and imaged by confocal microscopy. Upon addition of BCS, labile mitochondrial Cu^+ levels decrease by 36% relative to basal Cu^+ levels (Figure 4a, 4c), showing that Mito-CS1 can image basal levels of mitochondrial Cu^+ and detect depletions in this pool. In addition, nuclear staining with Hoechst 33342 confirms that the viability of HEK 293T cells is unaffected by the manipulation of cellular copper status (Figure 4a, 4b, 4c).

Finally, as an additional set of controls to corroborate that Mito-CS1 is detecting copper-dependent events, we performed analogous imaging studies with Rhodamine 123, a well established fluorescent marker for assaying mitochondrial membrane potential [88,89], under basal, copper-supplemented, and copper-depleted conditions. As described above, endogenous copper pools of HEK 293T cells were elevated with supplementation or depleted with chelation and then stained with 100 nM Rhodamine 123 (Figure 4e, 4f, 4g). The membrane potential as measured by Rhodamine 123 does not show statistically significant changes with either 300 μM $CuCl_2$ or 100 μM BCS treatment relative to control HEK 293T cells (Figure 4h), providing further evidence that Mito-CS1 is sensing changes in labile mitochondrial copper pools rather than reporting on mitochondrial membrane potential.

Mito-CS1 Imaging and ICP-OES Experiments Reveal that Mitochondrial Cu^+ Pools in *SCO1* and *SCO2* Patient Fibroblasts Are Comparable to Wildtype Counterparts

In our first application of Mito-CS1 as an analytical tool, we investigated whether the labile and total mitochondrial copper pools are affected by mutations in *SCO1* and *SCO2*, which are known to cause a severe copper deficiency at the cellular level in affected tissues and cell types.[36] We first evaluated the ability of Mito-CS1 to localize to mitochondria in human fibroblasts. As seen with HEK 293T cells, confocal microscopy of control fibroblasts stained with 5 μM Mito-CS1 for 15 min at 37 °C shows measurable levels of fluorescence in discrete subcellular locations (Figure 5a, Figure S2a). Co-staining experiments with MitoTracker Deep Red, a commercially available mitochondrial tracker (Figure 5b), BODIPY FL C_5-ceramide, a marker for the trans-Golgi (Figure 5c), and LysoTracker Green DND-26, a lysosomal maker (Figure S2b), establish that the observed fluorescence from Mito-CS1 is localized to mitochondria of these cells. Furthermore, nuclear staining with

NIH-PA Author Manuscript

NIH-PA Author Manuscript

NIH-PA Author Manuscript

Hoechst 33342 indicates that the cells are viable throughout the imaging experiments (Figure 5d, Figure S2c).

Analogous to the HEK 293T cells, we next tested how changes in global copper status affect the exchangeable mitochondrial copper pool in control fibroblasts. Control fibroblasts were grown in media supplemented with 300 μM and 500 μM $CuCl_2$ for 18 h and then stained with 5 μM Mito-CS1 for 15 min at 37 °C. The labile mitochondrial Cu^+ pool as visualized by Mito-CS1 is significantly expanded upon co-culture of fibroblasts with 500 μM $CuCl_2$ (Figure S3a, S3b, S3c). Staining with Rhodamine 123 does not show a statistically significant difference in the membrane potential between untreated and copper-supplemented fibroblasts (Figure S3d, S3e, S3f). Control fibroblasts treated with 100 μM BCS for 12 h and then stained with 5 μM Mito-CS1 for 15 min at 37 °C show a 45% decrease in mitochondrially-localized fluorescence intensity compared to their untreated counterparts (Figure 6a, 6b, 6c). The observed decrease in fluoresence intensity of Mito-CS1 in BCS-treated fibroblasts demonstrates that these cells possess a dynamic mitochondrial Cu^+ pool that is affected by changes in global copper status. In a set of parallel control experiments, Rhodamine 123 staining of control fibroblasts grown in normal media or media with 100 μM BCS for 12 h reveals no differences in membrane potential (Figure 6d, 6e, 6f) and nuclear staining with Hoescht 33342 shows that the cells are viable throughout the BCS treatment and imaging experiments (Figure 6a, 6b, 6c, 6d). COX activity is mildly reduced with 100 μM BCS treatment for 24 h (Figure 6g) but not sufficiently to affect the membrane potential (Figure 6e). Taken together, the data further establish that Mito-CS1 directly detects and responds to changes in endogenous mitochondrial Cu^+ levels in cultured human fibroblasts.

After establishing that Mito-CS1 can monitor the labile mitochondrial Cu^+ pool in control fibroblasts and sense dynamic changes in its size with alterations in copper status, we used this new chemical tool to characterize mitochondrial Cu^+ homeostasis in fibroblasts derived from patients with mutations in *SCO1* and *SCO2*. We also included fibroblasts derived from a patient with mutations in the copper exporter protein ATP7A in our analyses, for loss of ATP7A function in this cell type results in significant increases in total cellular copper content.[90,91] Control, *SCO1, SCO2*, and *ATP7A* patient fibroblasts were cultured for 48 h in growth medium, stained with 5 μM Mito-CS1 in DMEM, and imaged live by scanning confocal microscopy. Consistent with our findings using control fibroblasts, mutations in *ATP7A, SCO1* and *SCO2* do not affect the mitochondrial localization of Mito-CS1 or overall cell viability (Figure 7a, 7b, 7c, 7d). Interestingly, quantification of the Mito-CS1 fluorescence intensities reveals that the size of the labile mitochondrial Cu^+ pool is comparable in control, *SCO1* and *SCO2* patient fibroblasts, while it is significantly expanded in *ATP7A* patient fibroblasts (Figure 7e). We next used ICP-OES to measure total Cu at the whole cell and mitochondrial levels of organization in all four genetic backgrounds (Figure 7f). As expected, total cellular copper content is elevated in *ATP7A* patient fibroblasts and decreased in *SCO1* and *SCO2* patient fibroblasts when compared to control fibroblasts. In contrast, the total mitochondrial copper pool is only modestly altered in the patient backgrounds (Figure 7g), illustrating that this organelle more tightly controls its total and labile copper pools relative to the whole cell. Because the majority of mitochondrial copper is housed in the matrix and previous studies with competitor proteins, *in vitro* titrations and targeted chelators[31,69] argue that this pool is exchangeable, Mito-CS1 is likely visualizing this store within living cells. We performed two sets of additional control experiments to further support that Mito-CS1 is specifically reporting on a Cu^+-sensitive phenomenon in these patient fibroblasts. First, we used Rhodamine 123 staining to demonstrate that the mitochondrial membrane potential is maintained in both *SCO1* and *SCO2* patient backgrounds relative to the control (Figure 8a, 8b, 8c, 8d, 8e) Second, we measured COX activity in fibroblasts from all four genetic backgrounds (Figure 8f) to

NIH-PA Author Manuscript

NIH-PA Author Manuscript

NIH-PA Author Manuscript

confirm the presence of a severe COX deficiency in fibroblasts lacking functional SCO1 or SCO2. The collective data show that the observed changes in Mito-CS1 fluorescence are copper-dependent and are not an indirect consequence or non-specific phenomenon of differences across the cell lines in COX activity and/or membrane potential.

Finally, to support that the data obtained from *SCO1* and *SCO2* patient fibroblasts are representative of the observed *in vivo* phenotypes, we measured total copper content in crude mitochondria isolated from control, *SCO1* and *SCO2* patient livers by ICP-OES (Figure S4). As in cultured fibroblasts, the data show that the mitochondrial copper pool is not significantly altered in liver as a result of mutations in *SCO1* or *SCO2* (Figure S3a). While there was considerable variability in mitochondrial copper content across control liver samples, this observation can be explained by differences in total hepatocyte copper content (Figure S3b). Comparable copper levels in crude and highly purified mitochondria isolated from HEK 293T cells further suggest that the variation in mitochondrial copper levels observed across control liver samples is not simply a consequence of the isolation procedure (Figure S3a). Therefore, consistent with previously reported results[36] these data further suggest that fibroblasts are a competent disease model in terms of copper misregulation. Taken together, the combination of Mito-CS1 imaging and ICP-OES measurements patently shows that the mitochondrial copper store is a tightly regulated metal ion pool, as we observe little to no perturbation in the labile mitochondrial Cu^+ and total mitochondrial copper pools in *ATP7A, SCO1*, and *SCO2* patient fibroblasts compared to control congeners.

Concluding Remarks

In this report, we have described the synthesis, properties, and biological applications of Mito-CS1, a new targetable fluorescent probe that can selectively detect labile Cu^+ in mitochondria of living cells. Mito-CS1 is a unique Cu^+-specific small-molecule fluorescent indicator that features visible excitation and emission profiles, a turn-on response, and selectivity for Cu^+ over other abundant mitochondrial metal ions, including Fe^{2+}, Cu^{2+}, and Zn^{2+}. Confocal microscopy experiments with a model HEK 293T cell line and human fibroblasts establish that Mito-CS1 is chemically and spatially specific within living cells for mitochondrial Cu^+. Furthermore, we used Mito-CS1 in conjunction with biochemical and ICP metal analyses to monitor mitochondrial copper pools in *SCO* and *ATP7A* patient fibroblasts, cell lines that exhibit profound alterations in total cellular copper levels that mirror those observed in affected patient tissues *in vivo*. Interestingly, these experiments show that the mutations in question do not dramatically alter labile mitochondrial Cu^+ or total mitochondrial Cu pools relative to control cells, suggesting that cells maintain homeostatic control over mitochondria regulating copper homeostasis within a narrow window, to protect the main oxygen-consuming and energy-producing organelle relative to other areas of the cell. We anticipate that the Mito-CS1 reagent will find utility for future interrogations of how discrete copper handling pathways are organized into dynamic networks at the cell and systems levels of organization. In addition to applying Mito-CS1 for studies of mitochondrial copper biology, we are exploiting the modular probe scaffold to create new multifunctional probes for detecting Cu^+ and other biologically relevant analytes in discrete subcellular locales.

Experimental Section

Synthetic Materials and Methods

All reactions were carried out under a dry nitrogen atmosphere with flame-dried glassware. Silica gel P60 (SiliCycle) was used for column chromatography. Analytical thin layer chromatography was performed using SiliCycle 60 F254 silica gel (precoated sheets, 0.25 mm thick). Compound **1**[92], compound **10**[93], and Rhodamine 123[94] were synthesized

NIH-PA Author Manuscript

NIH-PA Author Manuscript

NIH-PA Author Manuscript

according to modified literature procedures. Compound **7**[60,61] was prepared according to previously reported procedures. HATU was purchased from ChemPep Incorporated (Wellington, FL). MitoTracker Deep Red, BODIPY FL C_5-ceramide, LystoTracker DND-26, and Hoechst 33342 were purchased from Invitrogen (Carlsbad, CA). All other chemicals were purchased from Sigma-Aldrich (St. Louis, MO) and were used as received. ^{1}H and ^{13}C NMR spectra were collected in $CDCl_3$, CD_3OD, and $(CD_3)_2SO$ (Cambridge Isotope Laboratories, Cambridge, MA) at 25 °C on a Bruker AVB-400 spectrometer at the College of Chemistry NMR Facility at the University of California, Berkeley. All chemical shifts are reported in the standard notation of parts per million using the peak of residual proton signals of $CDCl_3$ as an internal reference. Low-resolution mass spectral analyses were carried out using a 6130 quadrupole LC/MS 1200 Series (Aglient Technologies, Santa Clara, CA). High-resolution mass spectral analyses were carried out at the College of Chemistry Mass Spectrometry Facility at the University of California, Berkeley.

4-Hydroxy-2,6-dimethylbenzaldehyde (1)

Compound **1** was prepared according to a previously reported procedure with the following modifications: CH_3Cl_3 was passed over alumina and then added dropwise over 30 min to the reaction mixture. Characterization was consistent with that previously reported in the literature.[92]

Methyl 2-(4-formyl-3,5-dimethylphenoxy)acetate (2)

Methyl 2-bromoacetate (3.8 mL, 40 mmol) in anhydrous MeCN (60 mL) was added dropwise to a suspension of compound **1** (5.0 g, 33.3 mmol) and K_2CO_3 (9.19 g, 66.6 mmol) in MeCN (50 mL) at 60 °C. The resulting solution was heated at 60 °C for two days. The reaction mixture was cooled to room temperature and concentrated *in vacuo*. The crude reaction mixture was partitioned between water (100 mL) and EtOAc (3 × 100 mL). The organics were combined, dried over Na_2SO_4, filtered, and dried *in vacuo*. Diethyl ether (50 mL) was added to the crude solid and the resulting solid was collected via vacuum filtration and washed with diethyl ether (50 mL) to furnish compound **2** as an off-white solid (4.31 g, 58%). The reaction was repeated to generate more material for the subsequent reactions. ^{1}H NMR (400 MHz, $CDCl_3$): δ 2.59 (6H, s), 3.81 (3H, s), 6.58 (2H, s), 10.46 (1H, s). ^{13}C NMR (100 MHz, $CDCl_3$): δ 21.1, 52.5, 64.8, 115.3, 126.9, 144.6, 160.7, 168.8, 191.7. LRESI-MS calculated for [MH^+] 223.1, found 223.1.

Methyl 2-(4-(di(1*H*-pyrrol-2-yl)methyl)-3,5-dimethylphenoxy)acetate (3)

A solution of **2** (6.38 g, 28.7 mmol) in freshly distilled pyrrole (50.0 mL, 721 mmol) was wrapped in foil to protect it from light and purged with a stream of N_2 for five minutes. TFA (240 μL, 5.4 mmol) was then added dropwise, and the solution was stirred at room temperature for 1 h. After 1 h, TEA (1.0 mL, 7.2 mmol) was added and the reaction mixture continued to stir for 15 min. The reaction mixture was poured into toluene (150 mL) and washed with brine (2 × 100 mL). The organics were combined, dried over Na_2SO_4, filtered, concentrated to dryness and purified by flash chromatography two times (1st column: silica $CHCl_3$ to 0.1% MeOH in $CHCl_3$, 2nd column: silica, 0.5% EtOAc in CH_2Cl_2) to give a crude solid. Diethyl ether was added (3 × 20 mL), decanted, and the solid was collected via vacuum filtration and washed with diethyl ether (40 mL) to yield **3** as an off-white solid (1.81 g, 19%). ^{1}H NMR (400 MHz, $CDCl_3$): δ 2.08 (6H, s), 3.83 (3H, s), 4.62 (2H, s), 5.89 (1H, s), 5.99 (2H, s), 6.18 (2H, q, J = 2.8 Hz), 6.60 (2H, s), 6.67 (2H, br), 7.97 (2H, s). ^{13}C NMR (100 MHz, $CDCl_3$): δ 21.0, 38.1, 52.3, 65.1, 106.6, 108.7, 115.4, 116.3, 131.1, 131.2, 139.5, 156.3, 169.6. LRESI-MS calculated for [MH^+] 339.2, found 339.2.

NIH-PA Author Manuscript

NIH-PA Author Manuscript

NIH-PA Author Manuscript

(*Z*)-Methyl 2-(4-((5-chloro-1*H*-pyrrol-2-yl)(5-chloro-2*H*-pyrrol-2-ylidene)methyl)-3,5-dimethylphenoxy)acetate (4)

A solution of **3** (1.76 g, 5.2 mmol) in anhydrous THF (67 mL) was wrapped in foil to protect it from light and cooled to −78 °C. *N*-Chlorosuccinimide (1.53 g, 11.5 mmol) in anhydrous THF (20 mL) was wrapped in foil to protect it from light and was added dropwise in two portions via an addition funnel over the course of 15 min. The reaction was stirred for an additional 2 h at −78 °C, capped, and then placed in the freezer (−20 °C) overnight. The crude reaction mixture was poured into water (100 mL) at 0 °C and then extracted with CH_2Cl_2 (3 × 100 mL). The organics were combined, dried over Na_2SO_4, filtered, concentrated to dryness, and purified by flash chromatography (1st column: silica, 5% hexanes in CH_2Cl_2 to 5% MeOH in CH_2Cl_2, 2nd column: silica, 20% hexanes in CH_2Cl_2 to CH_2Cl_2) to provide the dichloro dipyrromethane as a crude red solid. This was carried onto the next step without further purification. *p*-Chloranil (1.30 g, 5.3 mmol) was added to a solution of the crude intermediate (1.05 g, 2.6 mmol) in CH_2Cl_2 (25 mL) and the reaction mixture continued to stir overnight at room temperature. The red-orange reaction mixture was concentrated to dryness and the residue was purified by flash chromatography (silica, 20% hexanes in CH_2Cl_2) afforded **5** as a dark orange solid (924 mg, 44% over two steps). ^{1}H NMR (400 MHz, $CDCl_3$): δ 2.08 (6H, s), 3.84 (3H, s), 4.67 (2H, s), 6.18 (2H, d, *J* = 4 Hz), 6.31 (2H, d, *J* = 4.4 Hz), 6.64 (2H, s). ^{13}C NMR (100 MHz, $CDCl_3$): δ 20.3, 52.4, 65.2, 113.3, 117.2, 128.1, 128.7, 138.2, 138.6, 138.9, 141.5, 157.6, 169.5. LRESI-MS calculated for [MH^+] 405.1, found 405.1.

3,7-Dichloro-5,5-difluoro-10-(4-(2-methoxy-2-oxoethoxy)-2,6-dimethylphenyl)-5*H*-dipyrrolo[1,2-*c*:2′,1′-*f*][1,3,2]diazaborinin-4-ium-5-uide (5)

Distilled DIEA (1.78 mL, 10.2 mmol) was added dropwise to a solution of **4** (924 mg, 2.3 mmol) in anhydrous CH_2Cl_2 (25 mL) and the resulting solution was allowed to stir for an additional 20 min. BF_3•OEt_2 (2.6 mL, 20.5 mmol) was then added dropwise over a period of 5 min, and the resulting solution was allowed to stir overnight. The reaction mixture was quenched with water (100 mL) and then extracted with CH_2Cl_2 (3 × 25 mL). The organics were combined, dried over Na_2SO_4, filtered, and dried *in vacuo*. Purification by flash chromatography (silica, 10% hexanes in CH_2Cl_2) gave **5** as a red-orange solid with a green luster (771 mg, 75%). ^{1}H NMR (400 MHz, $CDCl_3$): δ 2.06 (6H, s), 3.80 (3H, s), 4.65 (2H, s), 6.34 (2H, d, *J* = 4 Hz), 6.58 (2H, d, *J* = 4.4 Hz), 6.65 (2H, s). ^{13}C NMR (100 MHz, $CDCl_3$): δ 20.2, 52.3, 64.9, 113.6, 119.0, 123.3, 130.3, 134.2, 138.5, 143.1, 144.8, 158.2, 169.1. LRESI-MS calculated for [MH^+] 453.1, found 453.0.

3-Chloro-5,5-difluoro-7-methoxy-10-(4-(2-methoxy-2-oxoethoxy)-2,6-dimethylphenyl)-5*H*-dipyrrolo[1,2-*c*:2′,1′-*f*][1,3,2]diazaborinin-4-ium-5-uide (6)

A solution of **5** (771 mg, 17 mmol) in anhydrous THF (40 mL) was cooled to 0 °C and 25 wt% sodium methoxide (398 mg, 18.4 mmol) in anhydrous MeOH (90 mL) was added dropwise in two portions over 2.5 h. The reaction mixture was maintained at 0 °C for 4 h until the reaction was complete by TLC analysis. The solvent was removed *in vacuo*, and the resulting solid was partitioned between water (50 mL) and CH_2Cl_2 (3 × 50 mL). The organics were combined, dried over Na_2SO_4, filtered, and dried *in vacuo*. Purification by flash chromatography (silica, CH_2Cl_2) delivered **6** as a red-orange solid (640 mg, 84%). ^{1}H NMR (400 MHz, $CDCl_3$): δ 2.08 (6H, s), 3.83 (3H, s), 4.13 (3H, s), 4.65 (2H, s), 6.10 (1H, d, *J* = 4.8 Hz), 6.20 (1H, d, *J* = 4.0 Hz), 6.31 (1H, d, *J* = 4 Hz), 6.65 (2H, s), 6.70 (1H, d, *J* = 4.4 Hz). ^{13}C NMR (100 MHz, $CDCl_3$): δ 20.3, 52.4, 59.3, 65.1, 104.9, 113.5, 115.5, 124.8, 125.2, 130.7, 132.4, 133.9, 137.0, 139.0, 139.2, 158.0, 169.3, 169.6. LRESI-MS calculated for [MH^+] 449.1, found 449.1.

NIH-PA Author Manuscript

NIH-PA Author Manuscript

NIH-PA Author Manuscript

3-(Bis(2-((2-(ethylthio)ethyl)thio)ethyl)amino)-5,5-difluoro-7-methoxy-10-(4-(2-methoxy-2-oxoethoxy)-2,6-dimethylphenyl)-5*H*-dipyrrolo[1,2-*c*:2′,1′-*f*][1,3,2]diazaborinin-4-ium-5-uide (8)

Anhydrous MeCN (10 mL) was added to **6** (185 mg, 413 μmol) and **7** (575 mg, 1.8 mmol). The reaction mixture was purged with a stream of N_2 for five minutes and continued to stir at 45 °C in the dark for 72 h. The reaction mixture was concentrated to dryness. Purification by column chromatography (silica, 0.5% toluene in CH_2Cl_2 to 0.25% MeOH in CH_2Cl_2 to 0.5% MeOH in CH_2Cl_2) provided **8** as a red oil (168 mg, 56%). ^{1}H NMR (400 MHz, $CDCl_3$): δ 1.20 (6H, t, *J* = 7.4 Hz), 2.05 (6H, s), 2.53 (4H, q, *J* = 7.4 Hz), 2.70—2.74 (4H, m), 2.77—2.81 (4H, m), 2.86 (4H, t, *J* = 7.2 Hz), 3.79 (3H, s), 3.89 (4H, t, *J* = 7.4 Hz), 3.93 (3H, s), 4.62 (2H, s), 5.60 (1H, d, *J* = 4 Hz), 5.94 (1H, d, *J* = 4.8 Hz), 6.09 (1H, d, *J* = 3.6 Hz), 6.41 (1H, d, *J* = 4.8 Hz), 6.60 (2H, s). ^{13}C NMR (100 MHz, $CDCl_3$): δ 14.8, 20.2, 25.6, 30.1, 31.8, 32.2, 52.3, 53.3, 58.0, 65.0, 94.9, 110.0, 113.1, 121.7, 125.5, 126.8, 131.5, 133.0, 139.3, 157.3, 159.7, 161.6, 169.4. LRESI-MS calculated for [MH^+] 726.3, found 726.3.

3-(Bis(2-((2-(ethylthio)ethyl)thio)ethyl)amino)-10-(4-(carboxymethoxy)-2,6-dimethylphenyl)-5,5-difluoro-7-methoxy-5*H*-dipyrrolo[1,2-*c*:2′,1′-*f*][1,3,2]diazaborinin-4-ium-5-uide (Carboxy-CS1 9)

Powdered LiOH (20 mg, 833 μmol) was added to a solution of **8** (168 mg, 231 μmol) in anhydrous MeOH (3 mL) and anhydrous THF (3 mL) and the reaction mixture continued to stir overnight at room temperature. The reaction mixture was concentrated *in vacuo*, dissolved in water (15 mL), and the pH was adjusted to pH 1—2 with 0.5 M HCl. The reaction mixture was extracted with $CHCl_3$ (2 × 25 mL), the organics were combined, dried over Na_2SO_4, filtered, and dried *in vacuo*. Purification by column chromatography (silica, 1.5% MeOH in CH_2Cl_2 yielded **9** as a red oil (98 mg, 60%). ^{1}H NMR (400 MHz, $CDCl_3$): δ 1.24 (6H, t, *J* = 7.2 Hz), 2.10 (6H, s), 2.57 (4H, q, *J* = 7.2 Hz), 2.73—2.78 (4H, m), 2.81—2.85 (4H, m), 2.89 (4H, t, *J* = 7.2 Hz, *J* = 7.6 Hz), 3.93 (4H, t, *J* = 7.4 Hz), 3.97 (3H, s), 4.71 (2H, s), 5.64 (1H, d, *J* = 4.4 Hz), 5.96 (1H, d, *J* = 4.8 Hz), 6.13 (1H, d, *J* = 4 Hz), 6.45 (1H, d, *J* = 4.8 Hz), 6.66 (2H, s). ^{13}C NMR (100 MHz, $CDCl_3$): δ 14.8, 20.3, 26.0, 30.3, 31.7, 31.9, 32.2, 32.5, 53.3, 58.1, 64.7, 95.0, 110.1, 113.2, 121.8, 125.6, 127.2, 131.4, 131.6, 133.0, 139.6, 157.0, 159.8, 161.7, 173.6. LRESI-MS calculated for [MH^+] 712.2, found 712.2.

(2-Aminoethyl)triphenylphosphonium bromide (10)

Compound **10** was prepared according to a previously reported procedure with the following modifications: the crude solid was triturated with diethyl ether as reported but it was not further recrystallized from ethanol/diethyl ether as reported. The characterization data were consistent with results previously reported in the literature.[93]

Mitochondrial Coppersensor-1 (Mito-CS1, 11)

Compound **9** (98 mg, 137 μmol) and HATU (59 mg, 155 μmol) were dissolved in anhydrous CH_2Cl_2 (6 mL) and purged with a stream of N_2 for five minutes. After 20 min, **10** (59 mg, 153 μmol) was added in one portion and the reaction mixture continued to stir for 20 min. Distilled DIEA was added after 20 min and the reaction stirred at room temperature overnight. The reaction mixture was concentrated *in vacuo* and purified by column chromatography (1st column: silica, 0.25% EtOAc and 0.25% MeOH in CH_2Cl_2, 2nd column: silica, 0.5% EtOAc and 0. 5% MeOH in CH_2Cl_2, 3rd column: silica, 0.25% EtOAc and 0.25% MeOH in CH_2Cl_2 to 1% MeOH in CH_2Cl_2) to furnish **11** as a red semi-solid (67 mg, 48%). ^{1}H NMR (400 MHz, $CDCl_3$): δ 1.23 (6H, t, *J* = 7.2 Hz, *J* = 7.6 Hz), 2.07 (6H, s), 2.56 (4H, q, *J* = 7.4 Hz), 2.72—2.76 (4H, m), 2.80—2.84 (4H, m), 2.88 (4H, t, *J* = 7.4 Hz), 3.52 (2H, p, *J* = 7.2 Hz), 3.74 (2H, p, *J* = 6.4 Hz, *J* = 7.2 Hz), 3.91 (4H, t, *J* = 7.4 Hz), 3.95

NIH-PA Author Manuscript

NIH-PA Author Manuscript

NIH-PA Author Manuscript

(3H, s), 4.34 (2H, s), 5.62 (1H, d, J = 4 Hz), 5.95 (1H, d, J = 4.8 Hz), 6.11 (1H, d, 4 Hz), 6.45 (1H, d, J = 4.8 Hz), 6.71 (2H, s), 7.67—7.83 (15H, m). ^{13}C NMR (100 MHz, $CDCl_3$): δ 14.8, 20.2, 26.0, 30.3, 31.9, 32.4, 33.3, 53.3, 58.0, 66.6 95.0, 110.1, 113.4, 117.1, 117.9, 121.9, 125.7, 126.9, 130.7, 130.8, 133.4, 133.5, 135.5, 139.3, 156.9, 159.7, 169.5. HRESI-MS calculated for [M^+] 999.3576, found 999.3585.

Rhodamine 123

Rhodamine 123 was prepared according to a previously reported procedure with the following modifications: the crude solid was triturated with chloroform and the resulting solid was collected via vacuum filtration and washed with chloroform. Characterization was consistent with that previously reported in the literature.[94]

Spectroscopic Materials and Methods

Millipore water was used to prepare all aqueous solutions. All spectroscopic measurements were performed in phosphate buffered saline (1X PBS, pH 7.4, Invitrogen, Carlsbad, CA). Absorption spectra were recorded on a Varian Cary 50 spectrophotometer (Walnut Creek, CA) and fluorescence spectra were recorded using a Photon Technology International Quanta Master 4 L-format scanning spectrofluorometer (Lawrenceville, NJ) equipped with an LPS-220B 75-W xenon lamp and power supply, A-1010B lamp housing with integrated igniter, switchable 814 photon-counting/analog multiplier detection unit, and MD5020 motor driver. Samples for absorption and emission measurements were contained in 1-cm × 1-cm path length quartz cuvettes (1.4-mL volume, Starna, Atascadero, CA). Fluorescence quantum yields were determined by reference to rhodamine 101 inner salt in methanol (Φ = 1.0).[95] The binding affinity of Cu^+ to Mito-CS1 was measured using thiourea as a competitive ligand to provide a buffered Cu^+ solution. Stability constants for thiourea binding were taken from the literature $b_{12} = 2.0 \times 10^{12}$, $b_{13} = 2.0 \times 10^{14}$, $b_{14} = 3.4 \times 10^{15}$.[96]. Thiourea was delivered from an aqueous stock solution (200 mM, 500 mM). Cu^+ was delivered in the form of $[Cu(MeCN)_4[PF_6]]$ from an acetonitrile stock solution (1 mM, 5 mM). Excitation was provided at 540 nm and collected emission was integrated from 550 to 700 nm after 1 min or 2 min after the addition of dye or metal analyte. The apparent dissociation constant (K_d) was determined using the following equation: $(F - F_{min})/(F_{max} - F_{min}) = [Cu^+]/(K_d + [Cu^+])$, where F is the observed fluorescence, F_{max} is the fluoresence for the Cu^+:Mito-CS1 complex, F_{min} is the fluorescence for free Mito-CS1, and $[Cu^+]$ is the 'free' Cu^+ available for complexation, which was calculated using the stability constants for thiourea and standard competition equilibrium expressions. All other metal ions tested for metal ion selectivity studies with the exception of Fe^{2+} were from their chloride salts as aqueous solutions. Ammonium iron(II) sulfate hexahydrate was used as a source of Fe^{2+} and the salt was dissolved in degassed water.

Preparation of Cell Cultures

Cells were grown in the Tissue Culture Facility at the University of California, Berkeley with expert technical assistance from Ann Fischer and Michelle Yasukawa. HEK 293T cells were cultured in Dulbecco's Modified Eagle Medium (DMEM, Invitrogen, Carlsbad, CA) containing high glucose and without phenol red supplemented with GlutaMAX (Invitrogen, Carlsbad, CA) and 10% Fetal Bovine Serum (FBS, Hyclone, Logan, UT). Two days before imaging, cells were passed and plated on 12-mm glass coverslips coated with poly-L-lysine (50 mg/mL, Sigma, St. Louis, MO). Control, *ATP7A, SCO1*, and *SCO2* fibroblasts were cultured in Dulbecco's Modified Eagle Medium (DMEM, Invitrogen, Carlsbad, CA) containing high glucose and without phenol red supplemented with GlutaMAX (Invitrogen, Carlsbad, CA), 1 mM sodium pyruvate, and 10% Fetal Bovine Serum (FBS, Hyclone, Logan, UT). Two days before imaging, cells were passed and plated on 12-mm glass coverslips or 4-well chambered coverglass slides.

NIH-PA Author Manuscript

NIH-PA Author Manuscript

NIH-PA Author Manuscript

Cell Staining

For all experiments, solutions of Mito-CS1 (from 1 mM or 5 mM stocks in DMSO), CS3 (from 1 mM stocks in DMSO), Rhodamine 123 (from 50 μM stocks in DMSO), MitoTracker Deep Red (from a 50 μM stocks in DMSO), BODIPY FL C5-ceramide-BSA complex (from 1 mM stocks in water), and Hoechst 33342 (from a 5 mM stock in DMSO) were made in Dulbecco's Phosphate Buffered Saline with calcium chloride and magnesium chloride (DPBS, Invitrogen, Carlsbad, CA) or Dulbecco's Modified Eagle Medium without phenol red (DMEM, Invitrogen, Carlsbad, CA). For colocalization experiments control HEK 293T cells were incubated with 500 nM Mito-CS1 2.25 μM BODIPY FL C5-ceramide-BSA complex, 50 nM Mitotracker Deep Red, and 5 μM Hoechst 33342 for 15 min at 37 °C, 5% CO_2 in DPBS. Coverslips were then transferred to fresh DPBS for imaging. A similar procedure was followed for imaging with 500 nM Lysotracker Green DND-26. For copper and BCS treatments, 300 μM $CuCl_2$ or 100 μM BCS was added to the cells from a 0.1 mM aqueous stock solution one day prior to imaging. Cells were then incubated at 37 °C, 5% CO_2. After 18 hours, the media was exchanged for DPBS with 500 nM Mito-CS1 or 100 nM Rhodamine 123 and Hoechst 33342 and incubated for 15 min at 37 °C, 5% CO_2. Coverslips were then transferred to fresh DPBS for imaging. For colocalization experiments control fibroblasts were incubated with 5 μM Mito-CS1, 2.25 μM BODIPY FL C5-ceramide-BSA complex, and 5 μM Hoechst 33342 for 15 min at 37 °C, 5% CO_2 in DPBS. A similar procedure was followed for imaging with 250 nm Lysotracker Green DND-26 in DMEM. Coverslips were then transferred to fresh DPBS for imaging. MitoTracker Deep Red (50 nM in DPBS) was added on stage and then imaged. For BCS treatment, 100 μM BCS was added to the cells from a 0.1 mM aqueous stock solution one day prior to imaging. After 12 hours, the media was exchanged for DMEM with 5 μM Mito-CS1 or 100 nM Rhodamine 123 and 5 μM Hoechst 3342 and incubated for 15 min at 37 °C, 5% CO_2. Coverslips were then transferred to fresh DPBS for imaging. Similar procedures were followed for imaging changes in mitochondrial Cu^+ in the wild type, *ATP7A, SCO1*, and *SCO2* fibroblasts. For copper treatment, 300 μM or 500 μM $CuCl_2$ was added to the cells from a 0.1 mM aqueous stock solution one day prior to imaging. After 18 hours, the media in the chambered coverglass slides was exchanged for DMEM with 5 μM Mito-CS1 or 100 nM Rhodamine 123 and 5 μM Hoechst 3342 and incubated for 15 min at 37 °C, 5% CO_2, washed with fresh DPBS, and imaged in fresh DPBS. Control and *ATP7A* patient fibroblasts were stained with 2 μM CS3 and incubated for 10 min at 37 °C, 5% CO_2 in DPBS, washed with fresh DPBS, and imaged in fresh DPBS.

Fluorescence Imaging Experiments

Confocal fluorescence images were acquired at the Molecular Imaging Center at the University of California, Berkeley. Imaging experiments were performed with a Zeiss LSM510 META NLO Axioplan 2 laser-scanning microscope, a Zeiss 510NL META AxioIMAGER laser-scanning microscope, and a Zeiss LSM 710 laser-scanning microscope with a 40x or 63x water-immersion objective lens. Excitation of Mito-CS1 or CS3 loaded cells at 543 nm was carried out with a HeNe laser, and emission was collected using a META detector between 554—650 nm. Excitation of Lysotracker Green DND-26 at 488 nm was carried out with an Ar laser, and emission was collected using a META detector between 501—533 nm. Excitation of BODIPY FL C5-ceramide-BSA complex at 488 nm was carried out with an Ar laser, and emission was collected using a META detector between 498—511 nm. Excitation of Rhodamine 123 at 488 nm was carried out with an Ar laser, and emission was collected using a META detector between 501—576 nm. Excitation of MitoTracker Deep Red at 633 nm was carried out with a HeNe laser, and emission was collected using a META detector between 640—704 nm. Excitation of Hoechst 33342 was carried out using a MaiTai two photon laser at 780-nm pulses or a 405 nm diode laser and emission was collected between 469—522 nm with Rhodamine 123 and 447—533 nm for

NIH-PA Author Manuscript

NIH-PA Author Manuscript

NIH-PA Author Manuscript

all other dyes. ImageJ from the National Institutes of Health was used for analysis of the images. Specifically, the threshold for a field of cells was adjusted to select the pixels and was kept consistent in a given experiment. The selected pixels were analyzed for the median value. The mean of the median value for n fields of cells with standard error is reported and statistical analyses were performed with a two-tailed Student's *t*-test in Microsoft Excel.

ICP-OES analysis.[36]

Mitochondria and whole cells were digested in 40% nitric acid by boiling for 1 hr in capped, acid-washed tubes; samples were then diluted in ultra-pure, metal-free water; and analyzed by ICP-OES (PerkinElmer, Optima 3100XL). Acid-washed blanks were used as controls. Concentrations were determined from a standard curve constructed with serial dilutions of commercially available mixed metal standards (Optima). Error bars cannot be added to the data points for mitochondria isolated from *SCO1* and *SCO2* patient liver, owing to the scarcity of the material; the total tissue sample only consists of milligram quantities originating from a metabolic autopsy, thus precluding additional, large-scale analyses. Furthermore, we did not have access to liver samples from deceased *ATP7A* patients. To minimize any potential effects associated with experimental variability, mitochondria were isolated on the same day using identical buffers and reagents from each patient sample. Each sample was then split into two aliquots, and total mitochondrial copper content quantified in duplicate by ICP-OES in the same run.

Miscellaneous Procedures

COX and citrate synthase activities were measured in HEK 293T and fibroblast cell extracts as described elsewhere.[32,97] Protein concentration was measured by the Bradford method.[98]

Supplementary Material

Refer to Web version on PubMed Central for supplementary material.

Acknowledgments

We thank the Packard Foundation (C.J.C.), the Hellman Faculty Fund (C.J.C.), Amgen (C.J.C.), Astra Zeneca (C.J.C.), Novartis (C.J.C.), and the National Institute of General Medical Sciences (NIH GM 79465 to C.J.C., NIH GM 083292 to D.R.W.) for funding this work. C.J.C. is an Investigator with the Howard Hughes Medical Institute. We thank Holly Aaron (UCB Molecular Imaging Center) and Ann Fischer and Michelle Yasukawa (UCB Tissue Culture Facility) for expert technical assistance and helpful discussions.

References

1. Gray, HB.; Stiefel, EI.; Valentine, JS.; Bertini, I. Biological Inorganic Chemistry: Structure and Reactivity. 1st ed.. University Science Books; California: 2006.
2. Turski ML, Thiele DJ. J. Biol. Chem. 2009; 284:717–721. [PubMed: 18757361]
3. Banci L, Bertini I, Ciofi-Baffoni S, Kozyreva T, Zovo K, Paulmaa P. Nature. 2010; 465:645–648. [PubMed: 20463663]
4. Camakaris J, Voskoboinik I, Mercer JF. Biochem. Biophys. Res. Commun. 1999; 261:225–232. [PubMed: 10425169]
5. Rosenzweig AC, O'Halloran TV. Curr. Opin. Chem. Biol. 2000; 4:140–147. [PubMed: 10742187]
6. O'Halloran TV, Culotta VC. J. Biol. Chem. 2000; 275:25057–25060. [PubMed: 10816601]
7. Lee J, Marjorette MO, Nose Y, Thiele DJ. J. Biol. Chem. 2002; 277:4380–4387. [PubMed: 11734551]
8. Rees EM, Lee J, Thiele DJ. J. Biol. Chem. 2004; 279:54221–54229. [PubMed: 15494390]
9. Fontaine SL, Mercer JFB. Arch. Biochem. Biophys. 2007; 463:149–167. [PubMed: 17531189]
10. Davis AV, O'Halloran TV. Nat. Chem. Biol. 2008; 4:148–151. [PubMed: 18277969]

NIH-PA Author Manuscript NIH-PA Author Manuscript NIH-PA Author Manuscript

11. Kim B-E, Nevitt T, Thiele DJ. Nat. Chem. Biol. 2008; 4:176–185. [PubMed: 18277979]
12. Prohaska JR. Am. J. Clin. Nutr. 2008; 88:826S–829S. [PubMed: 18779302]
13. Kaplan JH, Lutsenko S. J. Biol. Chem. 2009; 284:25461–25465. [PubMed: 19602511]
14. Ma Z, Jacobsen FE, Giedroc DP. Chem. Rev. 2009; 109:4644–4681. [PubMed: 19788177]
15. Boal AK, Rosenweig AC. Chem. Rev. 2009; 109:4760–4779. [PubMed: 19824702]
16. Hass KL, Franz KJ. Chem. Rev. 2009; 109:4921–4960. [PubMed: 19715312]
17. White C, Lee J, Kambe T, Fritsche K, Petris MJ. J. Biol. Chem. 2009; 284:33949–33956. [PubMed: 19808669]
18. Barry AN, Shinde U, Lutsenko S. J. Biol. Inorg. Chem. 2010; 15:47–59. [PubMed: 19851794]
19. McRae R, Lai B, Fahrni CJ. J. Biol. Inorg. Chem. 2010; 15:99–105. [PubMed: 19865834]
20. Bertini I, Cavallaro G, McGreevy KS. Coord. Chem. Rev. 2010; 254:506–524.
21. Banci L, Bertini I, McGreevy KS, Rosato A. Nat. Prod. Rep. 2010; 27:695–710. [PubMed: 20442960]
22. Robinson NJ, Winge DR. Annu. Rev. Biochem. 2010; 79:537–562. [PubMed: 20205585]
23. Banci L, Bertini I, Cantini F, Ciofi-Baffoni S. Cell. Mol. Life Sci. 2010; 67:2563–2589. [PubMed: 20333435]
24. Rubino JT, Riggs-Gelasco P, Franz KJ. J. Biol. Inorg. Chem. 2010; 15:1033–1049. [PubMed: 20437064]
25. Cobine PA, Pierrel F, Winge DR. Biochim. Biophys. Acta. 2006; 1763:759–772. [PubMed: 16631971]
26. Pierrel F, Cobine PA, Winge DR. Biometals. 2007; 20:675–682. [PubMed: 17225062]
27. Horn D, Barrientos A. IUBMB Life. 2008; 60:421–429. [PubMed: 18459161]
28. Abriata LA, Banci L, Bertini I, Ciofi-Baffoni S, Gkazonis P, Spyroulias GA, Vila AJ, Wang S. Nat. Chem. Biol. 2008; 4:599–601. [PubMed: 18758441]
29. Leary SC, Winge DR, Cobine PA. Biochim. Biophys. Acta. 2009; 1793:146–153. [PubMed: 18522804]
30. Atkinson A, Winge DR. Chem. Rev. 2009; 109:4708–4721. [PubMed: 19522505]
31. Cobine PA, Pierrel F, Bestwick ML, Winge DR. J. Biol. Chem. 2006; 281:36552–36559. [PubMed: 17008312]
32. Leary SC, Kaufman BA, Pellecchia G, Guercin G, Mattman A, Jaksch M, Shoubridge EA. Hum. Mol. Genet. 2004; 13:1839–1848. [PubMed: 15229189]
33. Williams JC, Sue C, Banting GS, Yang H, Glerum DM, Hendrickson WA, Schon EA. J. Biol. Chem. 2005; 280:15202–15211. [PubMed: 15659396]
34. Horng YC, Leary SC, Cobine PA, Young FBJ, George GN, Shoubridge EA, Winge DR. J. Biol. Chem. 2005; 280:34113–34122. [PubMed: 16091356]
35. Matoba S, Kang JG, Patino WD, Wragg A, Boehm M, Gavrilova O, Hurley PJ, Bunz F, Hwang PM. Science. 2006; 312:1650–1653. [PubMed: 16728594]
36. Leary SC, Cobine PA, Kaufman BA, Guercin G, Mattman A, Palaty J, Lockitch G, Winge DR, Rustin P, Horvath R, Shoubridge EA. Cell Metabolism. 2007; 5:9–20. [PubMed: 17189203]
37. Banci L, Bertini I, Cavallaro G, Rosato A. J. Proteome Res. 2007; 6:1568–1579. [PubMed: 17300187]
38. Banci L, Bertini I, Ciofi-Baffoni S, Hadjiloi T, Martinelli M, Palumaa P. Proc. Natl. Acad. Sci. U.S.A. 2008; 105:6803–6808. [PubMed: 18458339]
39. Rigby K, Cobine PA, Khalimonchuk O, Winge DR. J. Biol. Chem. 2008; 283:15015–15022. [PubMed: 18390903]
40. Leary SC, Sasarman F, Nishimura T, Shoubridge EA. Hum. Mol. Genet. 2009; 18:2230–2240. [PubMed: 19336478]
41. Sung HJ, Ma W, Wang P, Hynes J, O'Riordan TC, Combs CA, McCoy JP Jr. Bunz F, Kang JG, Hwang PM. Nat. Commun. 2010; 1:1–8. [PubMed: 20975674]
42. Stiburek L, Zeman J. Biochim. Biophys. Acta. 2010; 1797:1149–1158. [PubMed: 20398622]
43. Leary SC. Antioxid. Redox Signal. 2010; 13:1403–1416. [PubMed: 20136502]

NIH-PA Author Manuscript

NIH-PA Author Manuscript

NIH-PA Author Manuscript

44. Banci L, Bertini I, Ciofi-Baffoni S, Kozyreva T, Mori M, Wang S. J. Biol. Inorg. Chem. 2011; 16:391–403. [PubMed: 21181421]
45. Papadopoulou LC, Sue CM, Davidson MM, Tanji K, Nishino I, Sadlock JE, Krishna S, Walker W, Selby J, Glerum DM, et al. Nat. Genet. 1999; 23:333–337. [PubMed: 10545952]
46. Jaksch M, Ogilvie I, Yao J, Hortenhaus G, Bresser HG, Gerbitz KD, Shoubridge EA. Hum. Mol. Genet. 2000; 9:795–801. [PubMed: 10749987]
47. Horvath R, Lochmüller, Stucka R, Yao J, Shoubridge EA, Kim SH, Gerbitz KD, Jaksch M. Biochem. Biophys. Res. Commun. 2000; 276:530–533. [PubMed: 11027508]
48. Valnot I, Osmond S, Gigarel N, Mehaye B, Amiel J, Cormeir-Daire V, Munnich A, Bonnefont JP, Rustin P, Rotig A. Am. J. Hum. Genet. 2000; 67:1104–1109. [PubMed: 11013136]
49. Jaksch M, Horvath R, Horn N, Auer DP, Macmillan C, Peters J, Gerbitz KD, Kraegeloh-Mann I, Muntau A, Karcagi V, Kalmanchey R, Lochmuller H, Shouebridge EA, Freisinger P. Neurology. 2001; 57:1440–1446. [PubMed: 11673586]
50. Jaksch M, Paret C, Stucka R, Horn N, Müller-Höcker J, Horvath R, Trepesch N.m, Stecker G, Fresinger P, Thirion C, Müller J, Lunkwitz R, Rödel G, Shoubridge EA, Lochmüller H. Hum. Mol. Genet. 2001; 10:3025–3035. [PubMed: 11751685]
51. Salviati L, Hernandez-Rosa E, Walker WF, Sacconi S, Dimauro S, Schon EA, Davidson MM. Biochem. J. 2002; 363:321–327. [PubMed: 11931660]
52. Hamza I, Giltin JD. J. Bioenerg. and Biomembr. 2002; 34:381–388. [PubMed: 12539965]
53. Foltopoulou PF, Zachariadis GA, Politou AS, Tsiftsoglou AS, Papadopoulou LC. Mol. Genet. Metab. 2004; 81:225–236. [PubMed: 14972329]
54. Stiburek L, Vesela K, Hansikova H, Pecina P, Tesarova M, Cerna L, Houstek J, Zeman J. Biochem. J. 2005; 392:625–632. [PubMed: 16083427]
55. Cobine PA, Pierrel F, Leary SC, Sasarman F, Horng Y, Shoubridge EA, Winge DR. J. Biol. Chem. 2006; 281:12270–12276. [PubMed: 16520371]
56. Leary SC, Mattman A, Wai T, Koehn DC, Clarke LA, Chan S, Lomax B, Eydoux P, Vallance HD, Shoubridge EA. Mol. Genet. Metab. 2006; 89:129–133. [PubMed: 16765077]
57. Banci L, Bertinin I, Ciofi-Baffoni S, Leontari I, Martinelli M, Palumaa P, Sillard R, Wang S. Proc. Natl. Acad. Sci. U.S.A. 2007; 104:15–20. [PubMed: 17182746]
58. Stiburek L, Vesela K, Hansikova H, Hulkova H, Zeman J. Am. J. Physiol. Cell Physiol. 2009; 296:C1218–C1226. [PubMed: 19295170]
59. Yang H, Brosel S, Acin-Perez R, Slavkovich V, Nishino I, Khan R, Goldberg IJ, Graziano J, Manfredi G, Schon EA. Hum. Mol. Genet. 2010; 19:170–180. [PubMed: 19837698]
60. Zeng L, Miller EW, Pralle A, Isacoff EY, Chang CJ. J. Am. Chem. Soc. 2006; 128:10–11. [PubMed: 16390096]
61. Miller EW, Zeng L, Domaille DW, Chang CJ. Nat. Protocols. 2006; 1:824–827.
62. Que EL, Chang CJ. J. Am. Chem. Soc. 2006; 128:15942–15943. [PubMed: 17165700]
63. Domaille DW, Que EL, Chang CJ. Nat. Chem. Biol. 2008; 4:168–175. [PubMed: 18277978]
64. Que EL, Domaille DW, Chang CJ. Chem. Rev. 2008; 108:1517–1549. [PubMed: 18426241]
65. Que EL, Chang CJ. Chem. Soc. Rev. 2010; 39:51–60. [PubMed: 20023836]
66. Que EL, Gianolio E, Barker SL, Aime S, Chang CJ. Dalton Trans. 2010; 39:469–476. [PubMed: 20023983]
67. Domaille DW, Zeng L, Chang CJ. J. Am. Chem. Soc. 2010; 132:1194–1195. [PubMed: 20052977]
68. Dodani SC, Domaille DW, Nam CI, Miller EW, Finney LA, Vogt S, Chang CJ. Proc. Natl. Acad. Sci. U.S.A. in press.
69. Yang L, McRae R, Henary MM, Patel R, Lai B, Vogt S, Fahrni CJ. Proc. Natl. Acad. Sci. U.S.A. 2005; 102:11179–11184. [PubMed: 16061820]
70. Wegner SV, Arslan H, Sunbul M, Yin J, He C. J. Am. Chem. Soc. 2010; 132:2567–2569. [PubMed: 20131768]
71. Taki M, Iyoshi S, Ojida A, Hamachi I, Yamamoto Y. J. Am. Chem. Soc. 2010; 132:5938–5939. [PubMed: 20377254]

NIH-PA Author Manuscript

NIH-PA Author Manuscript

NIH-PA Author Manuscript

72. Merchant SS, Allen MD, Kropat J, Moseley JL, Long JC, Tottey S, Terauchi AM. Biochim. Biophys. Acta. 2006; 1763:578–594. [PubMed: 16766055]
73. Robinson KM, Janes MS, Pehar M, Monette JS, Ross MF, Hagen TM, Murphy MP, Beckman JS. Proc. Natl. Acad. Sci. U.S.A. 2006; 103:15038–15043. [PubMed: 17015830]
74. Murphy MP, Smith RAJ. Annu. Rev. Pharmacol. Toxicol. 2007; 47:629–656. [PubMed: 17014364]
75. Ross MF, Prime TA, Abakumova I, James AM, Porteous CM, Smith RAJ, Murphy MP. Biochem. J. 2008; 411:633–645. [PubMed: 18294140]
76. Porteous CM, Logan A, Evans C, Ledgerwood EC, Menon DK, Aigbirhio F, Smith RAJ, Murphy MP. Biochim. Biophys. Acta. 2010; 1800:1009–1017. [PubMed: 20621583]
77. Dickinson BC, Chang CJ. J. Am. Chem. Soc. 2008; 130:9638–9639. [PubMed: 18605728]
78. Dickinson BC, Srikun D, Chang CJ. Curr. Opin. Chem. Biol. 2010; 14:50–56. [PubMed: 19910238]
79. Hardy M, Chalier F, Ouari O, Finet J, Rockenbauer A, Kalyanaraman B, Tordo P. Chem. Commun. 2007:1083–1085.
80. Hoye AT, Davoren JE, Wipf MP, Kagan VE. Acc. Chem. Res. 2008; 41:87–97. [PubMed: 18193822]
81. Biasutto L, Matarei A, Marotta E, Bradaschia A, Sassi N, Garbisa S, Zoratti M, Paradisi C. Bioorg. Med. Chem. Lett. 2008; 18:5594–5597. [PubMed: 18823777]
82. Ripke J, Zarse K, Ristow M, Birringer M. ChemBioChem. 2009; 10:1689–1696. [PubMed: 19492396]
83. Abu-Gosh SE, Kolvazon N, Tirosh B, Ringel I, Yavin E. Mol. Pharmaceutics. 2009; 6:1138–1144.
84. Yousif LF, Stewart KM, Kelley SO. ChemBioChem. 2009; 10:1939–1950. [PubMed: 19637148]
85. Loudet A, Burgess K. Chem. Rev. 2007; 107:4891–4932. [PubMed: 17924696]
86. Ulrich G, Ziessel R, Harriman A. Agnew. Chem. Int. Ed. 2008; 47:1184–1201.
87. Hamza I, Prohaska J, Gitlin JD. Proc. Natl. Acad. Sci. U.S.A. 2003; 100:1215–1220. [PubMed: 12538877]
88. Chen LB. Ann. Rev. Cell Biol. 1988; 4:155–81. [PubMed: 3058159]
89. Johnson LV, Walsh ML, Chen LB. Proc. Natl. Acad. Sci. U.S.A. 1980; 77:990–994. [PubMed: 6965798]
90. Bellingham SA, Lahiri DK, Maloney B, Fontaine SL, Multhaup G, Camakaris J. J. Biol. Chem. 2004; 279:20378–20386. [PubMed: 14985339]
91. Kaler SG. Nat. Rev. Neurol. 2011; 7:15–29. [PubMed: 21221114]
92. Yamada K, Toyota T, Takakura K, Ishimaru M, Sugawara T. New J. Chem. 2001; 25:667–669.
93. Maryanoff BE, Reitz AB, Duhl-Emswiler BA. J. Am. Chem. Soc. 1985; 107:217–226.
94. Ross JA, Ross BP, Rubinsztein-Dunlop H, McGeary RP. Synth. Commun. 2006; 36:1745–1750.
95. Karstens T, Kobs K. J. Phys. Chem. 1980; 84:1871–1872.
96. Martell, AE.; Smith, RM. Critical Stability Constants. Plenum Press; New York: 1989.
97. Capaldi RA, Marusich MF, Taanman JW. Methods Enzymol. 1995; 260:117–132. [PubMed: 8592440]
98. Bradford MM. Anal. Biochem. 1976; 72:248–254. [PubMed: 942051]

NIH-PA Author Manuscript

NIH-PA Author Manuscript

NIH-PA Author Manuscript

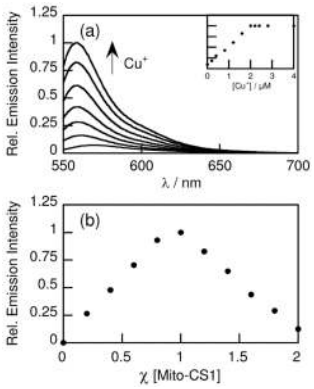

Figure 1.

Mito-CS1 responds to Cu^+ in an aqueous solution with 1:1 binding. (a) Fluorescence response of 2 μM Mito-CS1 to Cu^+. Spectra shown are for Cu^+ concentrations of 0, 0.2, 0.4, 0.8, 1.2, 1.6, 2.0, 2.2, 2.4, 2.8, and 4 μM. Spectra were acquired in PBS, pH 7.4, with 540 nm excitation. Inset, normalized fluorescence response (y-axis) of 2 μM Mito-CS1 to Cu^+. Spectra were acquired in PBS, pH 7.4. Excitation was provided at 540 nm and the integrated emission was collected from 550—700 nm. (b) Normalized Job's plot of Mito-CS1 and Cu^+. The total concentration of Mito-CS1 and Cu^+ were kept constant at 2 μM. Spectra were acquired in PBS, pH 7.4. Excitation was provided at 540 nm and emission intensity was measured at 558 nm.

NIH-PA Author Manuscript

NIH-PA Author Manuscript

NIH-PA Author Manuscript

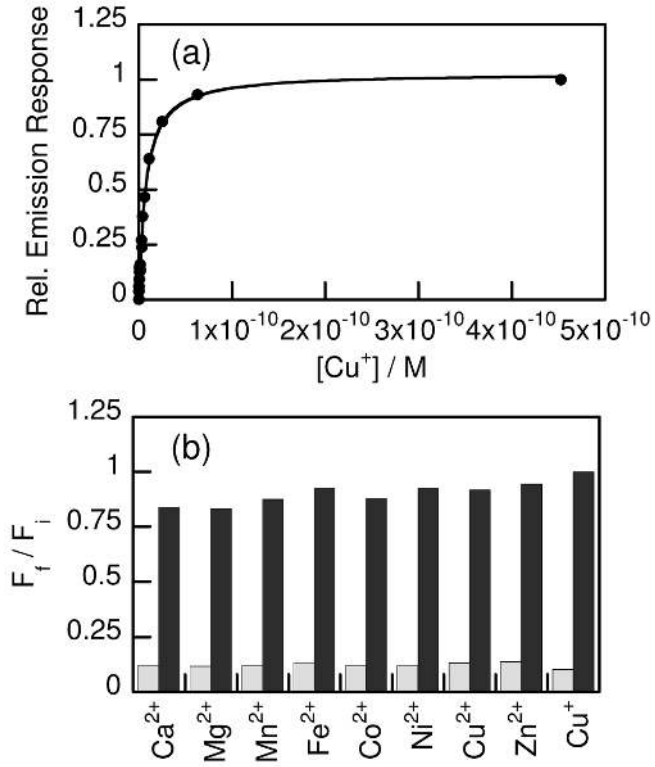

Figure 2.

Mito-CS1 can respond to a dynamic range of Cu^+ concentrations and is selective for Cu^+ over other biologically relevant metal ions. (a) Normalized fluorescence responses of 2 μM Mito-CS1 to thiourea buffered Cu^+ solutions for K_d value determination. Spectra were acquired in PBS, pH 7.4. Excitation was provided at 540 nm and the collected emission was integrated over 550—700 nm. The points shown are for free Cu^+ buffered at 0.10, 0.21, 0.45, 0.72, 0.91, 1.3, 1.4, 2.6, 3.0, 3.8, 6.1, 10.9, 25.1, 63.1, 452.5 pM, respectively. The observed K_d value is $7.2(3) \times 10^{-12}$ M. (b) Fluorescence responses of 2 μM Mito-CS1 to various metal ions. Bars represent the final (F_f) over the initial (F_i) integrated emission. Gray bars represent the addition of the competing metal ion (2 mM for Ca^{2+} and Mg^{2+}, 500 μM for Zn^{2+}, and 50 μM for all other cations) to a 2 μM solution of Mito-CS1. Black bars represent the addition of 2 μM Cu^+ to the solution. Spectra were acquired in PBS, pH 7.4. Excitation was provided at 540 nm, with emission integrated over 550—700 nm.

NIH-PA Author Manuscript
NIH-PA Author Manuscript
NIH-PA Author Manuscript

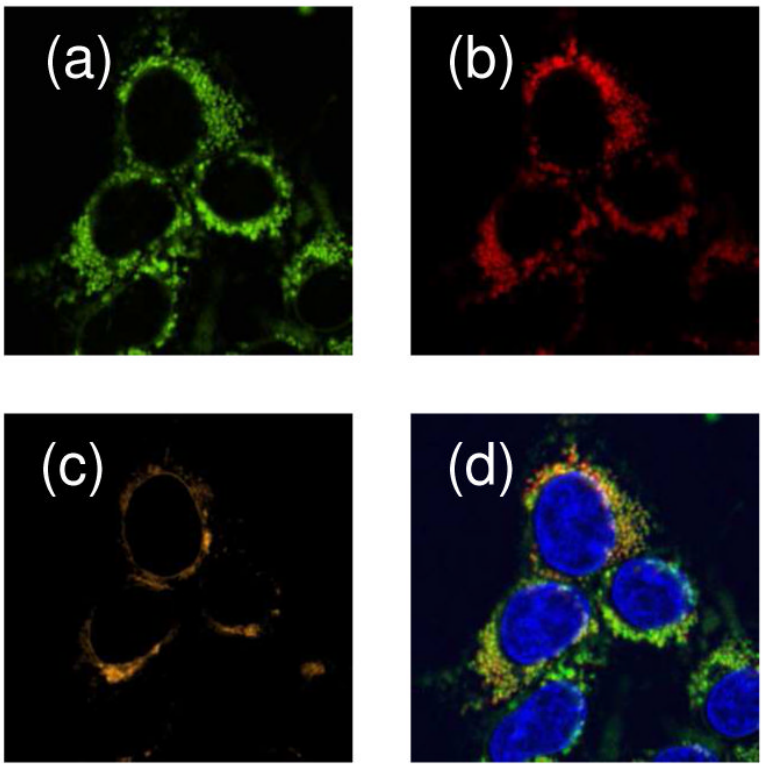

Figure 3.
Mito-CS1 colocalizes to mitochondria in live HEK 293T cells. HEK cells were stained with (a) 500 nM Mito-CS1, (b) 50 nM MitoTracker Deep Red, and (c) 2.25 μM BODIPY FL C5-ceramide-BSA complex and 5 μM Hoechst 33342 for 15 min at 37 °C in DPBS. (d) Overlay of (a) and (b) with Hoechst 33342.

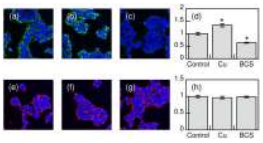

Figure 4.

Live-cell molecular imaging with Mito-CS1 and Rhodamine 123 reveals a labile mitochondrial Cu^{+} pool in HEK 293T Cells. (a) Control HEK cells, (b) HEK cells supplemented with 300 μM $CuCl_2$ in the growth medium for 18 h at 37 °C, and (c) HEK cells supplemented with 100 μM BCS in the growth medium for 18 h at 37 °C were stained with 500 nM Mito-CS1 and 5 μM Hoechst 33342 for 15 min at 37 °C in DPBS. (d) Plot of the mean fluorescence intensity of (a)—(c). Data were normalized to the control and statistical analyses were performed with a two-tailed Student's *t*-test (n = 4 fields of cells) relative to the control. $^{*}P < 0.01$ and error bars are ± s.e.m. (e) Control HEK cells, (f) HEK cells supplemented with 300 μM $CuCl_2$ in the growth medium for 18 h at 37 °C, and (g) HEK cells supplemented with 100 μM BCS in the growth medium for 18 h at 37 °C were stained with 100 nM Rhodamine 123 and 5 μM Hoechst 33342 for 15 min at 37 °C in DPBS. (h) Plot of the mean fluorescence intensity of (e)—(g). Data were normalized to the control, statistical analyses were performed with a two-tailed Student's *t*-test (n = 4 fields of cells) relative to the control, and error bars are ± s.e.m.

NIH-PA Author Manuscript NIH-PA Author Manuscript NIH-PA Author Manuscript

NIH-PA Author Manuscript

NIH-PA Author Manuscript

NIH-PA Author Manuscript

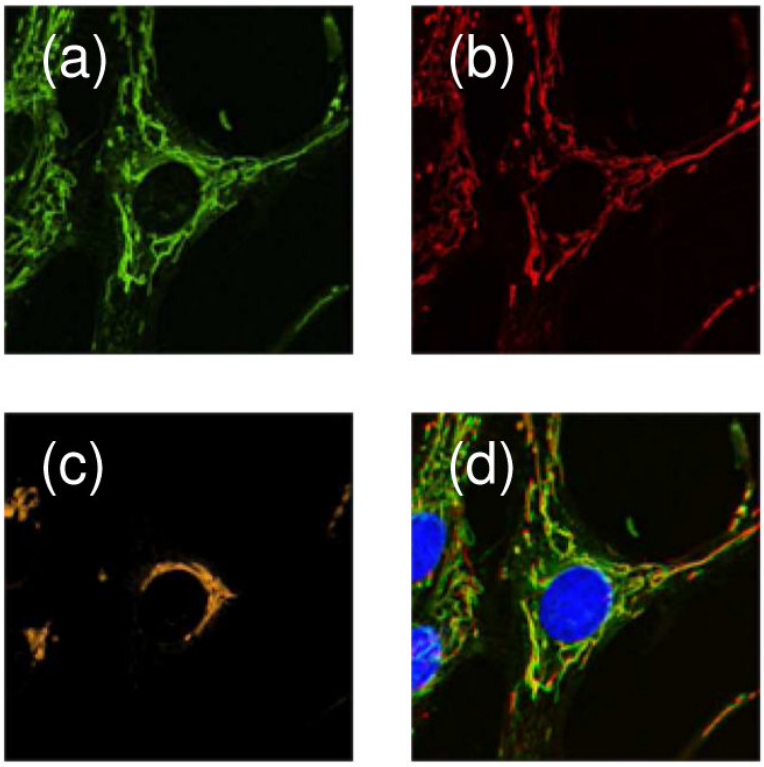

Figure 5.
Live-cell molecular imaging shows that Mito-CS1 colocalizes to mitochondria in a control cell line derived from human fibroblasts. Control fibroblasts were stained with (a) 5 μM Mito-CS1, (b) 50 nM MitoTracker Deep Red, (c) 2.25 μM BODIPY FL C5-ceramide-BSA complex and 5 μM Hoechst 33342 for 15 min at 37 °C in DPBS. (d) Overlay of (a) and (b) with Hoechst 33342.

NIH-PA Author Manuscript

NIH-PA Author Manuscript

NIH-PA Author Manuscript

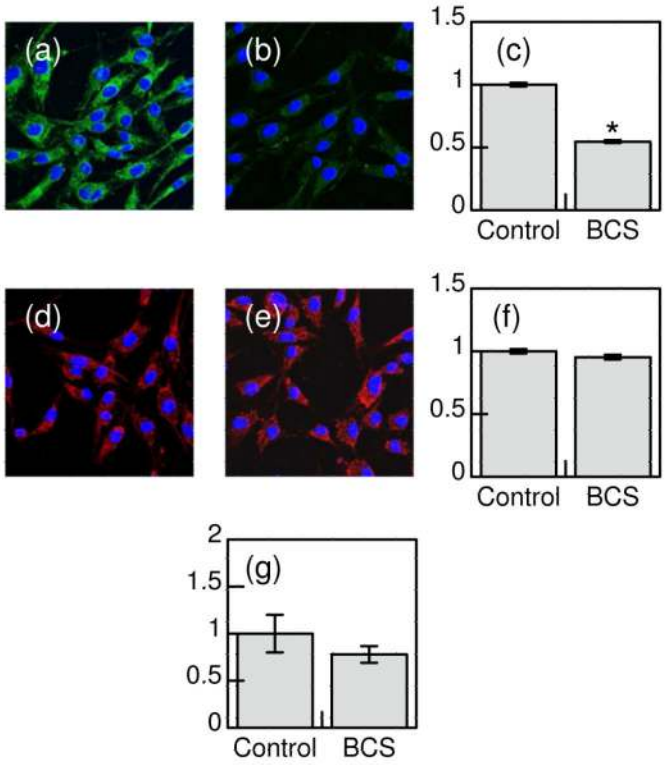

Figure 6.

Live-cell molecular imaging with Mito-CS1 and Rhodamine 123, biochemical approaches, and elemental analyses reveal that there is a dynamic mitochondrial Cu^{+} pool in a control cell line derived from human fibroblasts. (a) Control fibroblasts, (b) control fibroblasts supplemented with 100 μM BCS in the growth medium for 12 h at 37 °C were stained with 5 μM Mito-CS1 and 5 μM Hoechst 33342 for 15 min at 37 °C in DMEM. (c) Plot of the mean fluorescence intensity of (a) and (b). Data were normalized to the control and statistical analyses were performed with a two-tailed Student's *t*-test (n = 5 fields of cells). **P* < 0. 01 and error bars are ± s.e.m. (d) Control fibroblasts, (e) control fibroblasts supplemented with 100 μM BCS in the growth medium for 12 h at 37 °C were stained with 100 nM Rhodamine 123 and 5 μM Hoechst for 15 min at 37 °C in DMEM. (f) Plot of the mean fluorescence intensity of (d) and (e). Data were normalized to the control, statistical analyses were performed with a two-tailed Student's *t*-test (n = 5 fields of cells), and error bars are ± s.e.m. (g) COX activity[32,97] was measured in control fibroblasts and control fibroblasts supplemented with 100 μM BCS in the growth medium for 24 h. Data were normalized to the control, statistical analyses were performed with a two-tailed Student's *t*-test (n = 3), and error bars are ± s.e.m.

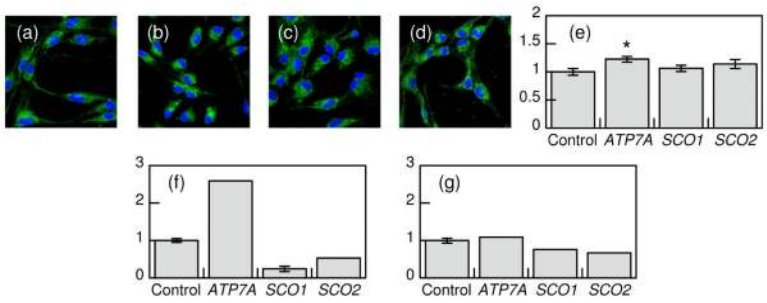

Figure 7.

Live-cell molecular imaging with Mito-CS1, biochemical approaches, and bulk metal ion analyses confirm that mutations in *SCO1* and *SCO2* do not significantly perturb the mitochondrial copper homeostasis. (a) Control fibroblasts, (b) *ATP7A* patient fibroblasts, (c) *SCO1* patient fibroblasts, and (d) *SCO2* patient fibroblasts were stained with 5 μM Mito-CS1 and 5 μM Hoechst 33342 for 15 min at 37 °C in DMEM. (e) Plot of the mean fluorescence intensity of (a)—(d). Data were normalized to the control and statistical analyses were performed with a two-tailed Student's *t*-test (n ≥ 4 fields of cells) relative to the control. $*P < 0.05$, and error bars are ± s.e.m. (f) Total copper levels were measured in control (n = 7), *ATP7A, SCO1* (n = 6) and *SCO2* patient fibroblasts and (g) mitochondrial copper levels were measured in control (n = 4), *ATP7A, SCO1* and *SCO2* patient fibroblasts by ICP-OES and are expressed as a fraction of the control using a previously described procedure.[36]

NIH-PA Author Manuscript NIH-PA Author Manuscript NIH-PA Author Manuscript

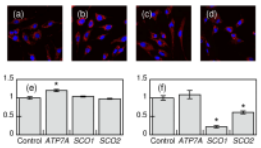

Figure 8.

Live-cell molecular imaging with Rhodamine 123 and biochemical approaches reveal that the membrane potential is preserved in COX-deficient fibroblasts derived from *SCO1* and *SCO2* patients. (a) Control, (b) *ATP7A*, (c) *SCO1*, and (d) *SCO2* patient fibroblasts were stained with 50 nM Rhodamine 123 and 5 μM Hoechst 33342 for 15 min at 37 °C in DMEM. (e) Plot of the mean fluorescence intensity of (a)—(d). Data were normalized to the control and statistical analyses were performed with a two-tailed Student's *t*-test ($n \geq 4$ fields of cells) relative to the control. $^{*}P < 0.01$ and error bars are ± s.e.m. (f) COX activity was measured in control, *ATP7A, SCO1* and *SCO2* fibroblasts using a previously described procedure.[32,97] Data were normalized to the control and statistical analyses were performed with a two-tailed Student's *t*-test ($n = 3$) relative to the control. $^{*}P < 0.01$ and error bars are ± s.e.m.

NIH-PA Author Manuscript NIH-PA Author Manuscript NIH-PA Author Manuscript

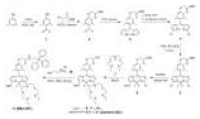

Scheme 1.

NIH-PA Author Manuscript

NIH-PA Author Manuscript

NIH-PA Author Manuscript